Soft Matter

Rheology and Dynamics of Solvent Segregation Driven Gel (SeedGel)

Journal:	*Soft Matter*
Manuscript ID	SM-ART-08-2022-001129.R1
Article Type:	Paper
Date Submitted by the Author:	06-Nov-2022
Complete List of Authors:	Xi, Yuyin; National Institute of Standards and Technology, ; University of Delaware, Murphy, Ryan; National Institute of Standards and Technology, NCNR Zhang, Qingteng; Argonne National Laboratory, X-ray Science Division Zemborain, Aurora; University of Chicago Narayanan, Suresh; e. Advanced Photon Source, Argonne National Laboratory, Argonne, IL 60439 USA, Chae, Junsu; Korea Advanced Institute of Science and Technology, Chemical & Biomolecular Engineering Choi, Siyoung; KAIST, Fluerasu, Andrei; Brookhaven National Laboratory, NSLS-II Wiegart, Lutz; Brookhaven National Laboratory, Photon Science Division Liu, Yun; National Institute of Standards and Technology,

Rheology and Dynamics of Solvent Segregation Driven Gel (SeedGel)

Yuyin Xi [1,2], Ryan P. Murphy [1], Qingteng Zhang [3], Aurora Zemborain [4], Suresh Narayanan [3], Junsu Chae [5], Siyoung Q. Choi [5], Andrei Fluerasu [6], Lutz Wiegart [6], Yun Liu [1,2*]

Email: yunliu@udel.edu or yun.liu@nist.gov

1. Center for Neutron Research, National Institute of Standards and Technology, Gaithersburg, MD, 20899, USA
2. Department of Chemical & Biomolecular Engineering, University of Delaware, Newark, DE, 19716, USA
3. X-ray Science Division, Argonne National Laboratory, Argonne, IL 60439, USA
4. Pritzker School of Molecular Engineering, University of Chicago, Chicago, IL 60637, USA
5. Department of Chemical and Biomolecular Engineering, Korea Advanced Institute of Science and Technology (KAIST), Daejeon 34141, Republic of Korea
6. National Synchrotron Light Source II, Brookhaven National Laboratory, Upton, New York 11973, United States

Abstract

Bicontinuous structures promise applications in a broad range of research fields, such as energy storage, membrane science, and biomaterials. Kinetically arrested spinodal decomposition is found responsible for stabilizing such structures in different types of materials. A recently developed solvent segregation driven gel (SeedGel) is demonstrated to realize bicontinuous channels thermoreversibly with tunable domain sizes by trapping nanoparticles in a particle domain. As the mechanical properties of SeedGel are very important for its future applications, a model system is characterized by temperature-dependent rheology. The storage modulus shows excellent thermo-reproducibility and interesting temperature dependence with the maximum storage modulus observed at an intermediate temperature range (around 28 ˚C). SANS measurements are conducted at different temperatures to identify the macroscopic solvent phase separation during the gelation transition, and solvent exchange between solvent and particle domains that is responsible for this behavior. The long-time dynamics of the gel is further studied by X-ray Photon Correlation Spectroscopy (XPCS). The results indicate that particles in the particle domain are in a glassy state

and their long-time dynamics are strongly correlated with the temperature dependence of the storage modulus.

Keywords:
Self-assembly; Nanoparticles; Binary Solvent; Rheology; Bicontinuous Structures; Colloidal Gel; Small-angle neutron scattering; X-ray Photon Correlation Spectroscopy.

Introduction

Colloidal gel has been a widely studied topic in soft matter research with applications in a wide range of fields, such as pharmaceutics, cosmetics, and tissue engineering. [1,2] The formed gel structures are usually process-dependent, rendering a wide range of opportunities for materials design and structure control. Colloidal systems in binary solvents, especially close to their critical point, exhibit rich phase behaviors and have been widely studied by many groups. [3–10] Understanding the self-assembly process of such systems is not only fundamentally important but also practically useful for various applications. [9–14]

During the past decade, colloidal gels with arrested bicontinuous channels gain tremendous attention due to their high specific surface area and interconnected channels with a wide range of applications, such as energy storage, membrane science, and biomaterials.[14–16] There are different ways to generate bicontinuous structures. [17–19] Among them, structures resulting from the kinetically arrested spinodal decomposition of a binary solvent using colloidal particles are emerging as a new research area. Bijel (bicontinuous interfacially jammed emulsion gel) is a widely studied example to stabilize such structures using colloidal particles that dislike both components of a binary solvent equally. [11,13,14,20]

Due to the importance of its application, the rheological behavior of Bijel has been studied. [21–23] It is found that the temperature plays an important role in controlling the rigidity of the material. [21]

Temperatures deeper into the 2-phase region (farther away from the critical temperature (T_c)) leads to a stronger gel. For the Bijel system in a binary solvent of water/ 2,6-lutidine (T_c = 34 ˚C), the storage modulus (G') drastically increases from ≈ 0.2 kPa at 40 ˚C (small quenching depth) to ≈ 3 kPa at 60 ˚C (large quenching depth). [21] The larger storage modulus with a temperature deeper in the 2-phase region is attributed to the stronger adsorption of particles at the interface between the two solvents. Also, the particle concentration is found to affect the mechanical properties of the Bijel. A higher concentration of particles results in a larger storage modulus. Scaling between the storage modulus and particle volume fraction (φ) of G' ≈ exp (32φ) is observed. [24] As the arrested particles in the percolated network are responsible for the mechanical strength, a higher concentration of particles would sharply increase the storage modulus. However, limited work has been reported to experimentally measure the dynamics of particles and correlate the dynamics with the rheological behaviors of Bijels.

Recently, a solvent segregation driven gel (SeedGel) has been developed and reported to stabilize bicontinuous channels. [9,10] The SeedGel is also prepared by dispersing nanoparticles in a binary solvent. However, different from Bijel systems, the nanoparticles in a SeedGel strongly favor one component of the binary solvent. Increasing the temperature increases a solvent-fluctuation introduced attraction that causes the particles aggregation, and eventually the formation of a SeedGel. A SeedGel has bicontinuous domains consisting of a particle domain and a solvent domain (solvent channel), as shown in Figure 1. During the gelation, the binary solvent in the system is also phase separated into two fluid domains. The particle domain coincides with the fluid domain with a high concentration of the solvent component favored by the particle surface, while the other fluid domain forms the solvent channel in a SeedGel. In our model system consisting of silica nanoparticles, water, 2,6-lutidine, water is the main component of the solvent in the particle

domain. The small inter-particle pores in the particle domain facilitate the macroscopic solvent phase separation between the solvent domain and particle domain. [25]

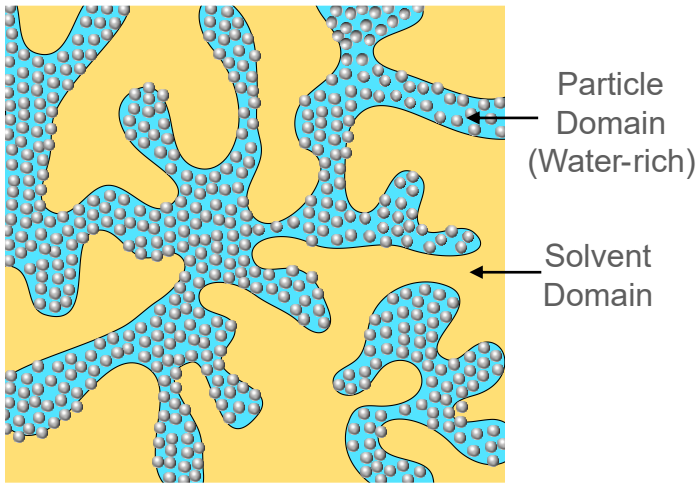

Figure 1. A schematic drawing shows the bicontinuous domains of SeedGel made of particle domain and solvent domain. In a model system of silica nanoparticles, water, and 2,6-lutidine, water is enriched in the particle domain and the 2,6-lutidine concentration in the solvent domain is higher than its nominal concentration in the sample. (The relative size of particles is not drawn to scale.)

The SeedGel is thermal reversible with great structure reproducibility. It even possesses some interesting optical properties, like dynamically tunable coloration.[8] However, its mechanical properties have not been examined. Here, a model SeedGel system is investigated to understand its temperature dependence on mechanical properties using a rheometer. It is found that its storage modulus first increases with the temperature. It reaches maximum strength at an intermediate temperature before the storage modulus decreases slowly by further increasing the temperature. Small angle neutron scattering (SANS) is used to investigate the solvent exchange between the particle domain and solvent domain during the gelation transition and in the gel state. And it is found that the solvent exchange plays an important role in the observed mechanical behavior. X-

ray Photon Correlation Spectroscopy (XPCS) experiments were further performed to study the long-time dynamics of the gel. And the long-time dynamics of particles in the gel state are found to be strongly correlated with the temperature dependence of the mechanical properties.

Materials and Methods

Materials:

Ludox TM-50 silica nanoparticle dispersion (Lot # MKCG0820) and Fomblin® Y (LVAC 06/6, averaged molecular weight 1800 g/mol, density 1.88 g/ml) were ordered from Sigma Aldrich (St Louis, MO). 2,6-lutidine was purchased from Tokyo Chemical Industry (TCI, Portland, OR). The chemicals were used as received.

SeedGel preparation:

The procedure for preparing SeedGel samples is the same as that in previous publications.[9,10] In short, the Ludox TM-50 silica nanoparticle dispersion is mixed with 2,6-lutidine at a pre-calculated concentration. The particle diameter is about 27 nm and the polydispersity is about 0.1.[9] The concentrations that result in the successful preparation of SeedGel are depicted in a phase diagram in our previous study.[10] The sample concentration used in this work is similar to those used in our previous work.[8–10] To prepare samples studied in this work, 300 μl 2,6-lutidine is added to every milliliter (ml) of Ludox TM nanoparticle dispersion. To ensure well-mixing, the sample is vigorously vortexed right after the addition of all components. It is then left on a roller to fully disperse the nanoparticles in the binary solvent with the application of a continuous low shear. Eventually, the sample becomes a well-mixed single-phase transparent liquid, which can be used to induce the formation of SeedGel by ramping up the temperature. The temperature during mixing and rolling is important for successfully preparing the sample. Too high of the temperature in the

process of mixing would cause macroscopic phase separation of the sample, rather than a one-phase homogeneous nanoparticle dispersion. A temperature of about 20 ˚C during mixing is used here to avoid bulk phase separation.

Small-angle neutron scattering (SANS) measurements:

The SANS experiments were conducted on the beamline of 30m NGB30 at the NIST Center for Neutron Research (NCNR, Gaithersburg, MD, USA). [26] Scattering data from three detector positions were stitched together to achieve a q-range of 0.001 $Å^{-1}$ < q < 0.461 $Å^{-1}$, where q is the magnitude of the scattering wave vector. Heating and cooling blocks driven by Peltier were utilized to control the temperature with a precision of ± 0.1 ˚C. The sample was loaded into a demountable Titanium cell with a path length of 1 mm. The body of the cell was made of Titanium and the windows of the cell were made of quartz. The cell was sealed with Teflon-coated O-rings. The scattering from a pair of quartz windows was measured and subtracted from the scattering results. An equilibration time of at least half an hour was allowed before each measurement when changing the sample temperature. The background noise level, the flux of the neutron beam, and transmission of each sample were recorded to convert the scattering intensity to an absolute intensity. All the data reduction was done with standard Igor (Wavemetrics, Portland, OR) macro. [27]

Rheology measurements:

Rheology measurements were performed on an Anton Paar MCR-301 rheometer with a cone-and-plate geometry. Tooling included a stainless-steel cone (50 mm diameter, 1-degree cone angle) and a temperature-controlled Peltier plate. After loading and trimming the sample into the geometry, the sample edge was immersed in an immiscible fluorinated oil (Fomblin Y) to prevent

the evaporation of volatile lutidine. When contained and immersed in the immiscible oil solvent trap, the sample viscosity remained constant at 15 ˚C over at least 24 hours, and the sample rheology continued to show thermo-reversible gelation throughout repeated heating and cooling cycles. This observation confirmed minimal loss of lutidine solvent and negligible oil entrainment. When the sample was not immersed in oil, the sample irreversibly gelled upon first heating and dried around the edges within 30 minutes.

Before each small amplitude oscillatory shear (SAOS) measurement, the sample was pre-sheared in the liquid state (15 ˚C) at a steady-shear rate of 20 s^{-1} for 5 minutes. This pre-shearing was sufficient to "erase" the rheological history in the sample before and after gelation, which was apparent from the consistent plateau in steady-shear viscosity before and after each SAOS measurement. After pre-shearing, the temperature was increased at approximately 2 ˚C/min to the target measurement temperature. The sample temperature was allowed to equilibrate for 5 minutes at rest before subsequent frequency sweep measurements.

Frequency sweeps were performed at a constant strain amplitude of 0.1 % strain, which was determined to provide sufficient torque signal while remaining within the linear viscoelastic regime for all examined sample temperatures (Figure S1 in the Supporting Information). After pre-shearing and sample equilibration, all frequency sweeps were first performed in direction of decreasing frequency from 100 rad/s to 0.1 rad/s with 8 points per decade, followed immediately by the reverse sweep from 0.1 rad/s to 100 rad/s. The consistent decreasing and increasing frequency sweeps indicated the sample did not sediment nor show time-dependent behavior during approximately 1 hour required for the frequency sweep.

Temperature ramps were performed immediately after initial pre-shearing at 15 ˚C and were performed at a fixed frequency (1 Hz), strain amplitude (0.1 %), and ramp rate (1 ˚C/min). The

heating ramp from 15 ˚C to 40 ˚C was followed immediately by the reversed temperature cooling ramp from 40 ˚C to 15 ˚C.

X-ray Photon Correlation Spectroscopy (XPCS):

The XPCS experiments were conducted at the 8ID beamline of the Advanced Photon Source (APS) at the Argonne National Laboratory (ANL).[28] The energy of the X-ray used was 11 keV and the flux was about 2.3×10^{10} photons per second. A relative bandpass of 0.03 % of full width at half maximum (FWHM) was used. [29] The beam size was defined as 15 μm × 6 μm. A rectangular detector with 256 pixels × 128 pixels was implemented to record the photons. The pixel size is 55 μm. The sample to detector distance is 4 m. SeedGel was loaded into a customized flat cell with a path length of about 1.5 mm. Kapton windows were used to confine the sample and the cell was sealed by O-rings. A few microliters of the liquid sample were enough to fill the cell. The small sample volume is advantageous in achieving a set temperature in a short time. The temperature control was achieved by QNW Peltier-controlled cuvette holders with an accuracy of ± 0.1 ˚C (Quantum Northwest, Liberty Lake, WA). Before each of the measurements, the temperature was cooled down to 7 ˚C and maintained for 2200 seconds to ensure full dissolution of the sample. Then it was heated up to the desired temperature to induce gelation of the sample. The ramping rate was fixed at 10 ˚C /min for all the temperatures. The recording of the results started 500 seconds after it first reached the set temperature, which provided enough time for the temperature equilibration. The measurements were repeated five times at different locations of the sample. The gel was then redissolved by cooling down to 7 ˚C with a cooling rate of 5 ˚C/min. The same procedure was repeated for a different temperature.

Fitting model of autocorrelation function from XPCS results:

The autocorrelation function can be fitted with a stretched exponential form, which is shown in Eq-1 below. [2]

$$g_2(q,t) = b\left[f_q e^{\left[-\left(\frac{t}{\tau}\right)^{\beta}\right]}\right]^2 + Bkg(q) \qquad \text{Eq-1}$$

where b is the optical contrast, which depends on the experimental setup and is used as a constant. During our analysis, b is determined to be 0.09 for our experiment with an independent experiment by measuring a sample without any dynamics within our q-ranges and time window. It is thus not a fitting parameter. f_q is the nonergodicity parameter and it is related to the plateau value at short times; τ is the terminal relaxation time, and β is the stretching exponent that is related to how fast the decay is. Here, *Bkg(q)* is the background value when the system loses correlation. Its theoretical value is 1. However, due to the finite pixel size on the area detector, *Bkg(q)* could deviate from 1, especially when the static scattering intensity, $I(q)$, changes sharply as a function of q. We developed a method to calculate *Bkg(q)* based on our 1-D SAXS results. This method is described in the next section. The largest deviation (about 0.005) from 1 is observed at the lowest q-range. Detailed calculations can be found in the Supporting Information. This method is useful for estimating the shift of background of the autocorrelation function for other samples too. The proposed numerical calculation from the SAXS profiles agrees well at low-q with the calculated results by approximating $I(q)$ as Cq^{-4} at low-q (Supporting information). As the deviation of the background occurs mainly in the low-q range, a small range of variation between 1 and 1.005 is allowed for *Bkg(q)* at q < 0.008 Å^{-1} for the fitting. The *Bkg(q)* is fixed to be 1 at higher-q values. f_q, τ, β are fitting parameters. All the fitting results are summarized in the Supporting Information.

Proposed theoretical approach to estimate the $g_2(q,\Delta t)$ background:

By recording the scattering intensity on a 2-D detector, the autocorrelation function $g_2(\Delta t)$ at a given q-position during an XPCS experiment can be calculated using "multi-speckle" analysis (Eq-2) as [28]

$$g_2(q,\Delta t) = \frac{\langle\langle I(t)I(t+\Delta t)\rangle_t\rangle_p}{\langle\langle I(t)\rangle_t\rangle_p\langle\langle I(\,t+\Delta t)\rangle_t\rangle_p} \quad \text{Eq-2}$$

Here, $I(t)$ is the intensity measured at time *t*. The symbol $\langle\rangle_t$ represents the averaged intensity over all time pairs with the time difference, Δt. And $\langle\rangle_p$ indicates the average of the intensity over the pixels within a certain range of q to improve the signal-to-noise ratio. The intensity correlation function, $g_2(q,\Delta t)$, is typically modeled using Eq-3:

$$g_2(q,\Delta t) = bg_1(q,t)^2 + Bkg(q) \quad \text{Eq-3}$$

where b is the optical contrast factor, and $g_1(q,t)$ is the intermediate scattering function.

Bkg(q) is the background of $g_2(q,\Delta t)$. Theoretically speaking, *Bkg(q)*$= 1$ for an ideal instrument. However, in practice, it can be larger than 1 due to the imperfection of a scattering instrument, and the inhomogeneity of the scattering intensity in a finite q-range when calculating $g_2(q,\Delta t)$ on an XPCS instrument. To fit the experimental data reliably, we propose here an approach to theoretically estimate *Bkg(q)* based on the average small-angle scattering data, $I(q)$. The background can be approximated as

$$Bkg(q) = 1 + \frac{\langle(I(q)-\langle I(q)\rangle_p)^2\rangle_p}{(\langle I(q)\rangle_p)^2} \quad \text{Eq-4}$$

The details are provided in the supporting information. The second term on the right-hand side of Eq-4 is determined by 1) the range of the magnitude of the scattering wave vectors used to calculate

$g_2(q,\Delta t)$; 2) the change of the scattering intensity $I(q)$ within this q range. The q range used for $\langle\rangle_p$ is determined by the instrument configuration and data calculation. Thus, based on obtained 2-D SAXS data, *Bkg(q)* can be theoretically calculated. In particular, for the isotropic scattering pattern, the calculation can be simplified by evaluating the value along the radial direction only.

Results and Discussion

Rheology

As demonstrated previously, the structures of this model SeedGel system can be reversibly formed by temperature-induced phase separation. [8–10] Rheology measurements are carried out to understand the mechanical properties of this model system at different temperatures. Here, the storage (G') and loss (G'') moduli are recorded as a function of temperature during the heating and cooling cycle (Figure 2 (a)). Consistent with the static structure, [8–10] the storage modulus is highly reproducible in response to the temperature change. Upon heating, the storage modulus increases sharply at around the gelation temperature and outweighs the loss modulus at around 26 ˚C (gelation temperature). This is consistent with the previous observation that above this same temperature, a solid gel with bicontinuous structures forms as evidenced by strong scattering intensity characterized by ultra-small angle neutron scattering (USANS). [9] This shows that the mechanical property of the gel is provided by the percolated particle domain. The gel transition temperature occurs at 26 ˚C. It is, in comparison, 8 °C lower than the critical temperature of the corresponding binary solvent (34 ˚C) with the same composition. Investigations on the equilibrium phase diagram of a similar system with lower particle concentrations than that used in this paper also showed consistent lower phase separation temperature than that of the bulk solvent. [30]

Even though it has been shown previously that the structure of the particle domain remains the same between 27 ˚C and 32 ˚C, [9,10] the mechanical properties of the gel vary with the temperature

within the same temperature range. The measured storage modulus increases with the temperature before reaching a maximum of about 3.4 kPa within an intermediate temperature around 28 ˚C. As a reference, the storage modulus ranges from tens of Pa to a few kPa for the bicontinuous domains formed by the Bijel approach. [5,7,31,32] The measured storage modulus of this model SeedGel system is on par with that of the strongest Bijels reported so far. Further increasing the temperature above ≈ 28 ˚C decreases the storage modulus of our sample. At temperatures above 36 ˚C, the storage modulus of SeedGel becomes comparable to the loss modulus. This indicates that temperature can be used to dynamically and reversibly control the mechanical properties of SeedGel. The storage modulus of this SeedGel shows non-monotonic dependence on the temperature.

Frequency sweeps at various temperatures are presented in Figure 2 (b). Above 25 ˚C, the storage modulus (G') exhibits weak frequency dependence, indicating a solid-like behavior. G' is slightly lower at 26 ˚C, compared to those at 28 ˚C and 30 ˚C. The modulus appears as almost a flat line between 28 ˚C and 30 ˚C within the frequency window probed. Interestingly, the storage modulus always increases with the oscillation frequency in Bijel systems, where neutrally wetted particles are jammed at the interface between two solvents. [5,7] A similar weak frequency dependence of G' is observed in a binary polymer blend. [33] At 34 ˚C the storage modulus is reduced and exhibits stronger dependence on frequency.

Figure 2 (c) shows frequency sweeps with finer temperatures between 24.75 ˚C and 27 ˚C. The storage modulus exhibits a power-law dependence with a slope of ½ at 25.5 ˚C. The power-law slope of ½ is known to be a characteristic feature at the gelation point. [34,35] Remarkably, the frequency sweep curves of G' and G" can be scaled to a single master curve with one scale factor of α_T over more than 10 decades of scaled frequency. (Figure 2 (d)) The scale factor is defined

with reference to the moduli at 26 ˚C (T_{ref}) with the relationship $\alpha_T = e^{\left(-7\times10^5\times\left(\frac{1}{T}-\frac{1}{T_{ref}}\right)\right)}$. This is often referred to as Time-Temperature Superposition (TTS), which indicates that the gel structures evolve in a self-similar manner. [36,37] TTS is extremely useful for expanding the frequency range and predicting the sample response beyond which can be measured by conventional rheometry. [38] It is often encountered in polymeric systems. [38] In colloidal samples, similar scaling behaviors are reported in carbon black gels, [36,39] fumed silica gels, [39] Laponite gels, [40] and aluminosilicate gels. [37] In SeedGel, the storage modulus (G') gradually increases after gelation and the loss modulus shows a local minimum before it starts to decrease (Figure 2 (d)), which has been observed in aluminosilicate gels. [37]

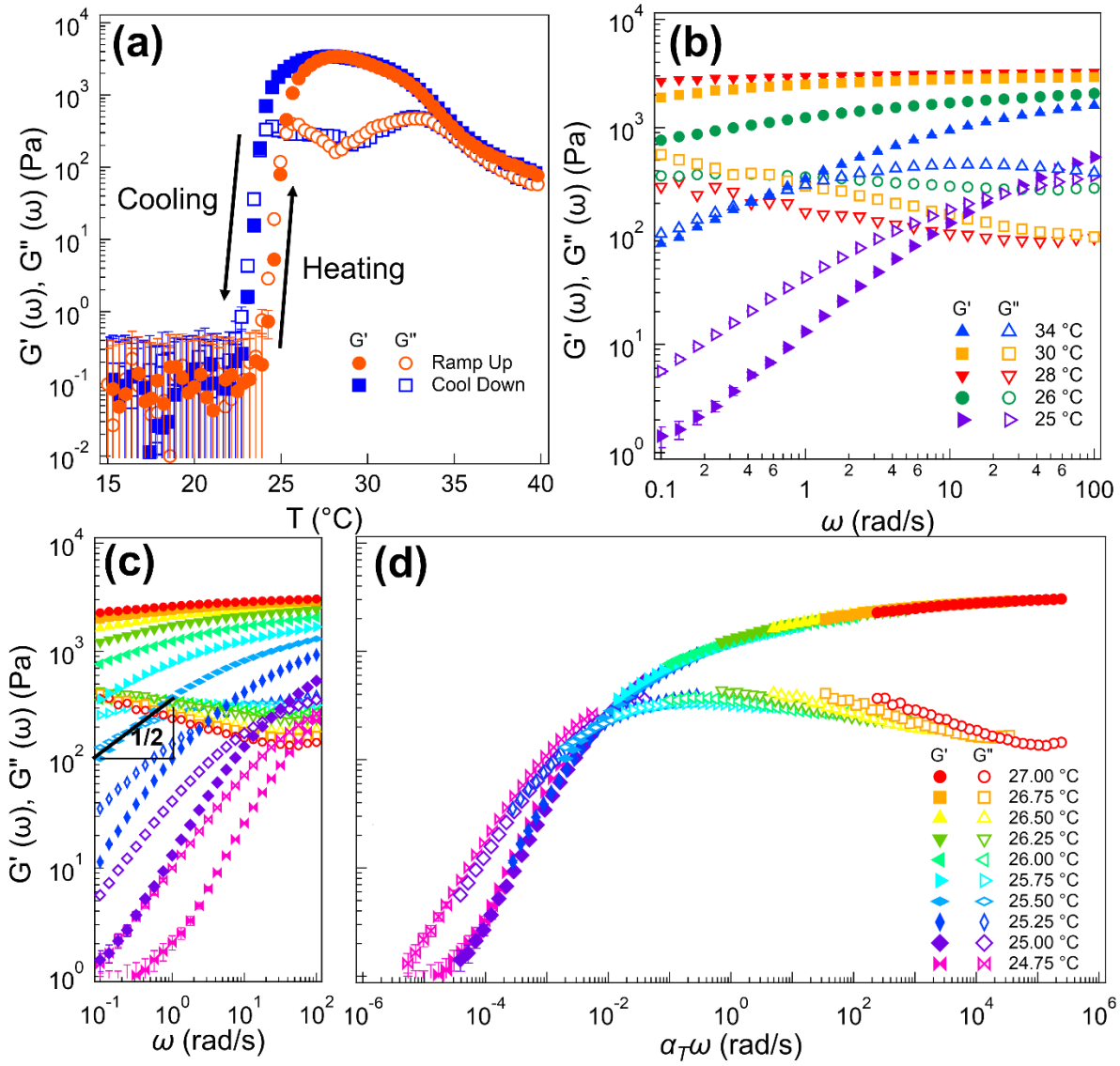

Figure 2 (a) Storage and loss moduli of SeedGel by small amplitude oscillatory shear measurements at different temperatures with a constant shear strain of 0.1 % and constant angular frequency of 1 rad/s. (b) and (c) Storage and loss moduli as a function of angular frequency at a constant shear strain of 0.1 % at different temperatures. Frequency sweeps in (b) and (c) were obtained by ramping up the sample to a target temperature at about 2 ˚C/min after sufficient pre-shearing at 15 ˚C. (d) Master curve of storage and loss moduli for different temperatures as a function of normalized frequency. The error bars in the data are estimated from the torque uncertainties of the rheometer.

The temperature dependence of the storage modulus of this SeedGel is quite interesting and is dramatically different from that of Bijel. The mechanical strength of Bijel is observed to increase continuously with the increasing temperature. [21] This is reasonable as the elastic behavior of a Bijel is mainly determined by the interfacial tension between domains. The fact that the storage modulus of our SeedGel increases first and then decreases later when continuously increasing the temperature indicates that the mechanisms are more complicated and are likely determined by multiple factors that compete with each other. To further understand the structural and dynamic origin of the temperature dependence of the storage modulus, we studied this SeedGel system with both SANS and XPCS.

SANS experiments are performed within the same temperature range. The sudden jump of the low-q intensity ($q < 0.004$ Å^{-1}) at about 25 ˚C shown in Figure 3 (a) indicates the onset of large bicontinuous domain formation that is consistent with the gelation temperature observed by the rheological measurement shown in Figure 2. Thus, the gelation is indeed due to the formation of the large-scale bicontinuous structure. The formation of the particle domain causes the sharp increase of the storage modulus around the gelation temperature. As discussed previously, the particle domain has both water-rich solvent and charged nanoparticles (Figure 1). Both of those two components in the particle domain are not thermodynamically favored by the solvent domain. The majority of lutidine resides in the solvent domain. It has been experimentally demonstrated that interfacial tension between water and 2,6-lutidine increases upon heating due to reduced miscibility. [41]

Since the particle domain and the solvent domain become more and more thermodynamically incompatible with each other at higher temperatures, it is thus expected that heating up the sample increases the mechanical strength, which is consistent with the observed experimental result under

about 28 ˚C. However, a different mechanism must be introduced to explain the reduced storage modulus at temperatures higher than 28 ˚C.

It is noted that the SANS intensity slightly changes at the low-q value ($q < 0.004$ Å^{-1}) through the gel state. This is not due to the structural change of the particle domain but is mainly due to the contrast change of the two domains. This is supported by our SAXS experiments that the structures of the particle domains are almost identical during the temperature range between 28 ˚C and 36 ˚C (Figure S2 in the Supporting Information). Since SAXS is mostly sensitive to nanoparticles in our sample, this confirms that structures formed by nanoparticles remain the same during the gel state across the studied temperature range. This small intensity change at low-q of the SANS patterns in the gel state is thus mainly due to the solvent exchange, altering the averaged scattering length density (SLD) of both domains simultaneously. More explanations are presented in the Supporting Information. In the particle domain, the main solvent component is water, and all the nanoparticles are arrested in the particle domain. In the solvent domain, both water and 2,6-lutidine exist, but there are no particles based on the experimental results from previous studies. [8,9,42,43] (Detailed discussions are included in the supporting information.) When the sample is heated up, the water concentration is increased in the particle domain and decreases in the solvent domain, which affects the contrast between the two domains. The composition change of the solvent molecules in both domains is likely playing an important role in affecting the storage modulus of the SeedGel.

To better understand the solvent composition change in the particle domain, we quantitatively analyzed the peak intensity of the SANS data at 0.04 Å^{-1} in the high-q region (Figure 3 (b)) which is mainly related to the form factor of the spherical particles.[9] As the particle shape and concentration remain constant for the sample upon temperature variation, the intensity change at $q = 0.04$ Å^{-1} is a direct result of solvent composition variation, which modifies the contrast between

particles and the surrounding medium. Detailed explanations are shown in the supporting information. Figure S3 ~ Figure S6 in the Supporting Information shows the validity of the interpretation of the intensity changes at q = 0.04 $Å^{-1}$ as the contrast change between the particles and the surrounding solvent. To track the change of the solvent composition as a function of temperature, the intensities at high-q (0.04 $Å^{-1}$) are plotted against temperature in Figure 3 (b). To clearly identify the gel transition temperature of the same sample, the intensity at low-q (0.0013 $Å^{-1}$) is also plotted in Figure 3(b) for comparison.

The increase of intensity in the high-q region (around q > 0.023 $Å^{-1}$) is mainly due to the solvent composition change in the vicinity of particles in the particle domain when increasing the temperature. It is important to point out that the contrast in the high-q region comes from the SLD difference between the nanoparticles and their surrounding solvent. This is different from the contrast between the two domains at low-q values. The neutron SLD of silica, water, and 2,6-lutidine is 3.48×10^{-6} $Å^{-2}$, -0.56×10^{-6} $Å^{-2}$, and 1.16×10^{-6} $Å^{-2}$, respectively. In the liquid state (20 ˚C), the contrast is mostly due to the SLD difference between silica and the binary solvent.

When the SeedGel is formed, water is enriched in the particle domain as most 2,6-lutidine is partitioned into the solvent domain. This leads to an increase in the SLD difference between silica particles and the solvent of the particle domain at elevated temperatures. As a result, the scattering intensity at high-q increases due to the change in the solvent environment around nanoparticles. Interestingly, a sudden jump at high-q around 25 ˚C coincides with the gelation temperature. This change in the contrast is due to the phase separation of the binary solvent between the particle domain and solvent domain. In this process, the water-rich solvent phase stays in the particle domain. Note that the phase separation temperature of the bulk binary solvent of water and 2,6-lutidine occurs around 34 ˚C at this solvent composition. However, the particles in the particle

domain form small pores that facilitate the macroscopic solvent phase separation at a much lower temperature (26 ˚C) than that of the bulk phase separation temperature of this binary solvent. Based on our previous SANS results with contrast matching, the silica nanoparticles mostly stay within the particle domain enriched with water [9] because the particle surface strongly favors water. [44] The favorable wetting of water on the particle surface causes the phase separation of the solvent and the accumulation of water within the nanopores formed by the closely packed silica nanoparticles. [25] This is the first direct experimental observation to confirm that the macroscopic phase separation temperature of the binary solvent in the SeedGel occurs at the gelation temperature even though this has been speculated previously. Note that before the gel transition, there are already microscopic phase transitions of the binary solvent that induce the attraction between the particles causing them to percolate into the large particle domains. Once the particle domains form, they promote and arrest the macroscopic phase separation of the binary solvent.

The possible effect on the scattering intensity change caused by the thermal expansion of 2,6-lutidine and water is also investigated. And it is concluded that solvent exchange is still the main reason that leads to the change of the scattering intensity with the temperature at both q = 0.0013 $Å^{-1}$ and q = 0.04 $Å^{-1}$. The estimated magnitude of the SLD difference due to density change between 22 ˚C and 38 ˚C is less than one order of magnitude compared to that caused by the exchange of the solvent. [41] In addition, the estimation also shows that the thermal expansion of the solvent only increases the contrast between the particle domain and the solvent domain, rather than decreases it as indicated by the SANS results in the low-q region. Thus, the change in intensity results primarily from the solvent exchange between domains at low-q. At temperatures above 25 ˚C, the intensity at high-q continues increasing with the temperature. This is direct experimental evidence that the water concentration in the particle domain keeps rising at elevated temperatures.

The continued enrichment of water in the particle domain persists up to 38 ˚C. Due to the mass balance, the solvent composition in the solvent domain also changes accordingly with a continuously decreasing water concentration. Even though the particle domain structure and particle packing have almost no change as evidenced by the SAXS experiment results shown in Figure S2 in the supporting information, their dynamics could be affected by the exchange of the solvent molecules. Since the silica particles are highly charged and strongly favor water over lutidine, the presence of some lutidine in the solvent of the particle domain may slow down its dynamics. It has been shown that reducing the lutidine concentration results in a lowered viscosity of the binary solvent.[45] Increasing the temperature increases the water concentration and decreases the lutidine concentration in the solvent of the particle domain. Together with the slightly lower solvent viscosity at high temperatures, this favors the faster motions of the particles. The faster motions of particles in the particle domain could result in a weaker gel.

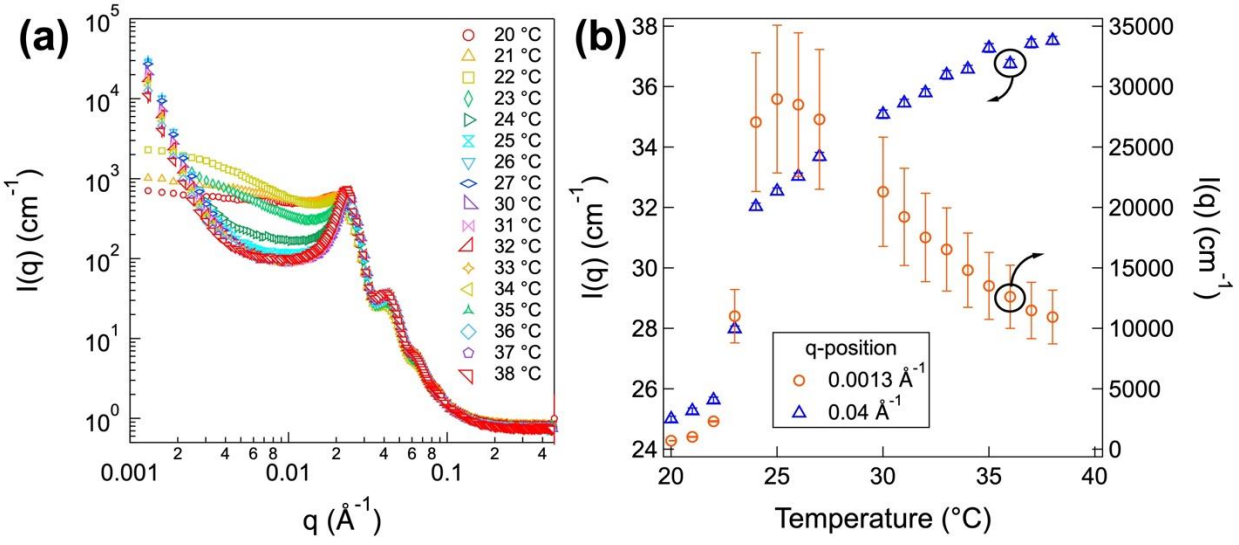

Figure 3 (a) SANS profiles of SeedGel at the temperature range between 20 ˚C and 38 ˚C. (b) The intensities as a function of temperature at q = 0.0013 Å^{-1} and q = 0.04 A^{-1}. The error bars represent one standard deviation.

To better understand the slow dynamics of silica particles of this SeedGel sample and its temperature-dependent property, the system is further investigated with X-ray photon correlation spectroscopy (XPCS) at three temperatures within the gel region, 26 ˚C, 30 ˚C, and 34 ˚C. Those temperatures correspond to three states in the gel: near the gelation point, temperature with the highest storage modulus, and temperature with reduced modulus, respectively. It is important to note that XPCS probes smaller length scales compared to rheology measurements that characterize macroscopic mechanical properties of the sample. In XPCS experiments, a series of the 2-D scattering pattern from the sample is recorded as a function of time. The summation of all the frames throughout measurements results in small-angle X-ray scattering (SAXS) profiles shown in Figure 4. The XPCS experiments cover the dynamics associated with a wide range of length scales, including dynamics related to the domains (low-q) and that of the particles (high-q). It is important to note that the scattering intensities of X-rays from our samples are mainly due to the structures formed by silica nanoparticles. Similar to what is observed in the SANS results (Figure 3 (a)), a peak at around 0.023 $Å^{-1}$ in Figure 4 is related to the well-repeated inter-particle distance due to high electrostatic charges on the particle surface. Within the probed temperature range, this peak does not show any change in the q-position, indicating that the solvent exchange between domains does not affect the particle packing. At intermediate q-range ($0.006\ Å^{-1} < q < 0.02\ Å^{-1}$) and the low-q region ($q < 0.006\ Å^{-1}$), the scattering profile at 26 ˚C shows slight deviation from those at higher temperatures. This small difference agrees with our previous report that the domain size of SeedGel slightly above the gelation temperature is larger than that formed at higher temperatures. [9,10] It is consistent with the relatively weak strength of SeedGel around the gelation temperature (Figure 2). [9,10] The curves at 30 ˚C and 34 ˚C are almost identical to each other at this q-range, suggesting a similar packing of particles at those temperatures. Consistent with SANS

data in Figure 3, an upturn in the low-q intensity with a dependence of q^{-4} is observed in SAXS results, which indicates the formation of bicontinuous domains with a smooth interface.

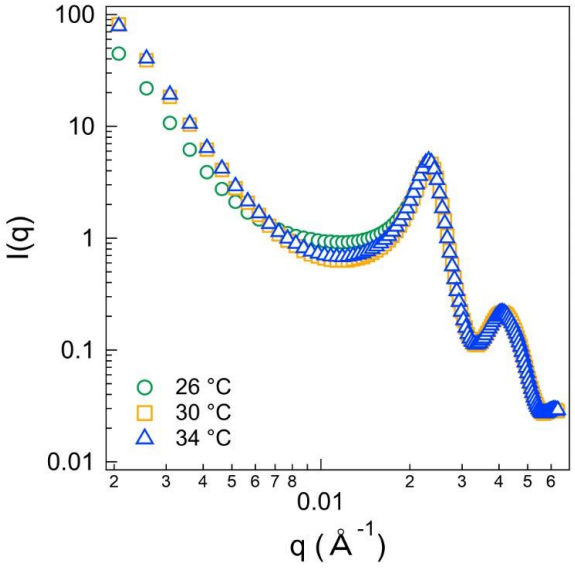

Figure 4 Small-angle X-ray scattering profiles of SeedGel at 26 ˚C, 30 ˚C, and 34 ˚C.

The static structures resolved by SANS and SAXS identify the q-positions that are relevant to both the domains and the nanoparticles. To capture the relevant dynamics, the XPCS experiments are conducted at different temperatures. The autocorrelation function g_2 is plotted as a function of delay time, Δt, at three different temperatures in Figure 5.

Representative $g_2(q,t)$ curves at q-positions of 0.003 $Å^{-1}$ and 0.023 $Å^{-1}$ are selected to show in Figure 5 (a) and Figure 5 (b), which characterize dynamics that correspond to the motions of the domains and particles, respectively. At each temperature, the measurements are repeated multiple times and they exhibit a similar temperature-dependent trend (Figure S7 in the Supporting Information). For all the curves, the correlation function shows a plateau value at short delay times

and gradually decreases to approximately 1 at longer delay times where there is no correlation between frame pairs. Note that the SAXS data do not change over the course of each XPCS measurement as shown by Figure S8 in the Supporting Information indicating that the structures of the sample do not change during the experiment.

At all temperatures, the g_2 plateau values at q = 0.003 Å^{-1} are clearly larger than those at q = 0.023 Å^{-1}. This is because a faster time decay outside the probing window exists for the dynamics of nanoparticles (q = 0.023 Å^{-1}). The decay of g_2 also occurs at a longer time scale at q = 0.003 Å^{-1} when compared to its corresponding g_2 values at q = 0.023 Å^{-1}. This is attributed to the fact that larger domains (lower q-values) move slower than small particles (larger q-values). It is important to note that relaxation time at q = 0.023 Å^{-1} is on the order of tens of seconds, which is at least three orders of magnitude slower than that of freely moving particles with similar sizes in the same binary solvent. The dynamics of nanoparticles in SeedGel are at least two orders of magnitude slower than those for particles arrested in reversible aggregates. [46,47] Those aggregates are formed in similar binary solvent mixtures with lower particle concentrations near the critical temperature (volume fraction of 8 % or 2 %). [46,47] It suggests that the nanoparticles in SeedGel are highly immobile. When comparing different temperatures, the initial plateau value of the autocorrelation function at 26 ˚C starts from a lower value in both low-q and high-q positions compared with that of the results at higher temperatures. It is because the particles and domains at this temperature are not as fully arrested as those at higher temperatures. The initial decay is too fast to be captured within the time window of the XPCS experiments. Such multi-step decay is also observed for other colloidal gels. [48] The slightly fast dynamics of particles at 26 ˚C explain our previous observation that the static structures right around the gelation temperature are relatively weak. [10] The rheology

results in Figure 2 also reflect the smaller storage modulus around the gelation temperature when compared to that at 30 ˚C.

Not only the plateau values of g_2 curves, but the relaxation time also shows a strong dependence on temperature in SeedGel. A longer relaxation time is observed at 30 ˚C while increasing or decreasing the temperature would accelerate the decay time. This indicates that the particle domain becomes less rigid at 26 ˚C and 34 ˚C, which corroborates with the rheology data in Figure 2. The slowest dynamics at 30 ˚C correspond to the largest storage modulus within this temperature range (Figure 2).

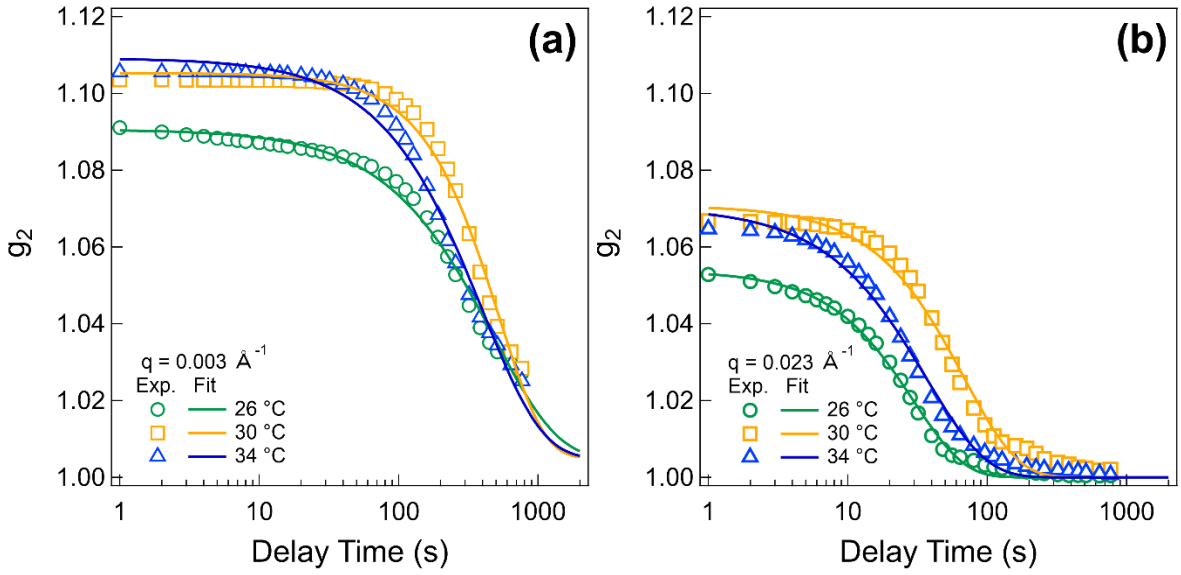

Figure 5 Comparison of autocorrelation function $g_2(q, t)$ as a function of delay time at different temperatures: 26 ˚C, 30 ˚C, and 34 ˚C. The represented curves are plotted at two different q-positions: (a) q = 0.003 Å^{-1} and (b) q = 0.023 Å^{-1}. The plotted error bars are smaller than the symbols.

To obtain a quantitative description of the dynamics, the autocorrelation functions are modeled with a stretched exponential form. The details of the fitting are described in the method section. Due to the finite pixel size of the detector, extra steps are taken to correct a deviation from 1 of the

autocorrelation function background. A method to calculate the deviation from the scattering profile is developed and explained in detail in the Supporting Information (Figure S9). All the fitting results are plotted in the Supporting Information Figure S10 ~ Figure S13. The fitting results of the autocorrelation functions are plotted in Figure 6 to Figure 7. Figure 6 compares the wavevector dependence of the nonergodicity parameters (f_q) obtained at different temperatures. The nonergodicity parameter is related to the plateau value of g_2 at short times. Note that $f_q = 1$ if there are no motions in the studied sample at the corresponding q range. However, if $f_q < 1$, it means that there are some fast motions so fast that could not be measured by the current instrument setup. As the shortest correlation time for our experiment setup is about 1 s, this fast motion has a timescale faster than 1 s.

The results in Figure 6 imply that both space-spanning interconnected bicontinuous domains and the nanoparticles are structurally arrested. At all temperatures, the f_q values approach 1 when q is getting close to 0.003 Å^{-1}. It indicates that there are no domain motions with a moving distance comparable to the length scale ($\frac{2\pi}{q} \approx 200$ nm) probed by this q-value at the time scale of one second. As the domain size of the particle domain is about a few micrometers, this indicates that the formed particle domains are rigid (without movement in length scales comparable to the domain size). When increasing the q value, the measurement begins to be sensitive to the motions with a shorter distance. The sample has different f_q values at different temperatures at q = 0.0046 Å^{-1} (corresponding to the length scale of ≈ 130 nm). Though f_q at 30 ˚C and 34 ˚C remains to be one, f_q at 26 ˚C is about 0.73. Hence, a significant amount of particles at this temperature have motions with a distance comparable to 130 nm with a correlation time of less than one second. Consistent with the rheological measurement shown in Figure 2 (b), the sample is softer at 26 ˚C

than that at higher temperatures. Overall, f_q at 30 ˚C and 34 ˚C are almost identical across the whole q-range. But the results at 26 ˚C are smaller for all q-values indicating that there are more fast motions (faster than one second) at this temperature than that at high temperatures. The increase of the nonergodicity parameter as a function of temperature is also observed in a system using a similar binary solvent but with a high particle concentration. [49] To make sure that the observed results are the same across the whole samples, Figure S10 in the Supporting Information shows the reproducible trend from fitted f_q at different positions in our sample at the three temperatures.

At higher q-values (i.e. q = 0.023 $Å^{-1}$ or larger), the measurement is not sensitive to the domain motions anymore. It is mainly due to the motions of particles motions inside the particle domain. Thus, the XPCS measurements allow us to understand the dynamics of particles inside the particle domain. The results show direct evidence that the particles in the particle domain are already in a glassy state. The SeedGel formation is thus due to the glass formation in the particle domain. This agrees with the physical picture of SeedGel that particles are jammed into the particle domain that percolates throughout the sample volume. Clear peaks of f_q are shown near the static structure factor peak widely exist in many other colloidal gel systems. [2,6,49,50]

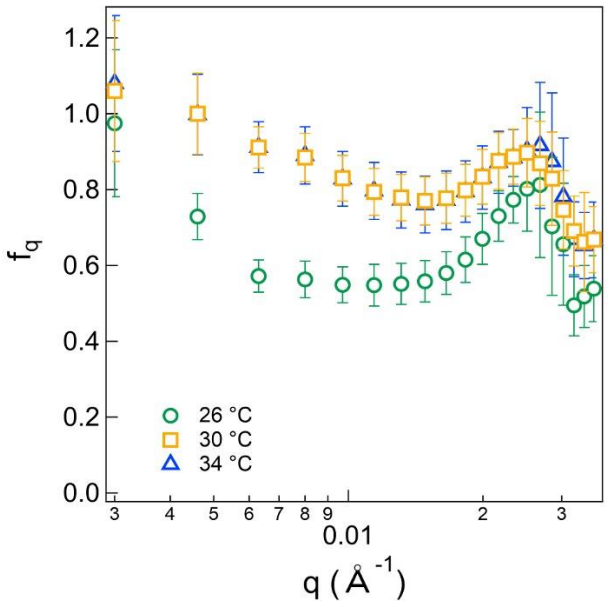

Figure 6 Nonergodicity parameter as a function of wavevector at different temperatures. The error bar represents one standard deviation.

The decay in the system can be quantitatively described by the relaxation time (τ). Their values are obtained from the fitting of Eq-4 and are plotted against the wavevector in Figure 7 at different temperatures. The relaxation time is close to 1000 seconds at a low-q value and decreases with the increase of the wavevector. Compared to the system with a lower particle concentration (8 %), the relaxation time of particles in SeedGel is about five orders magnitudes slower at qR $\approx$ 1 at 26 °C. [4] The fitting of the linear region in a log-log plot in Figure 7 reveals a $\tau \sim q^{-1}$ dependence, which has been reported in different colloidal gels. [2,51–53] The power-law dependence of q^{-1} on τ has been attributed to the local stress in a colloidal glass. [53,54] At around 0.023 Å^{-1}, a slow-down of the relaxation time appears at q-values corresponding to the structure factor peak at all temperatures. This is known as the de Gennes narrowing phenomenon, which has been observed in colloidal gels and protein solutions. [2,51,55] Different from f_q, the relaxation time is larger at 30 ˚C at all q-positions. Therefore, the motions of the system are the slowest at 30 ˚C. The relaxation time

becomes smaller at both 26 ˚C and 34 ˚C. This is again consistent with a larger storage modulus at 30 ˚C. As similar particle packing is observed for SeedGel at this temperature range (Figure 3 and Figure 4), it further confirms that solvent composition (segregation) plays an important role in determining the dynamics of particles. The results measured at multiple sample locations rule out the possibility that this difference is caused by the heterogeneity of the sample (Figure S11 in the Supporting Information). It is noted that the relaxation time decreases with the temperature near the bulk solvent critical point in our SeedGel sample, which is in contrast to a glass forming sample with higher nanoparticle concentrations (49 %), where the relaxation time increases with temperature near the critical point. [49] Even though both systems use the binary solvent and silica particles, the two systems are fundamentally different. In our system, our particles are much smaller with a diameter of about 27 nm. As a result, the particle in the particle domain has water rich solvent due to the small pore size induced macroscopic solvent phase separation. In comparison, the diameter of silica particles is about 400 nm in the previous study. [49] The pore size between particles is significantly larger than that in our case and may result in a different behavior of the binary solvent mixed with the silica particles. In addition, due to the small particle size (about 27 nm), there is a strong long range electrostatic repulsion between particles. And the relative range of the attraction between particles is larger than the typical range of the short-range attraction system close to the gelation temperature based on a previous study. [56] However, in the previous system [49], the interaction potential between particles can be successfully modeled with a short-range attraction (≈ 49%). The particle size could affect the interaction ranges, which could potentially change the structures and mechanical properties of SeedGel. An on-going study on the effect of particle size on rheological behavior and dynamics of SeedGel is underway.

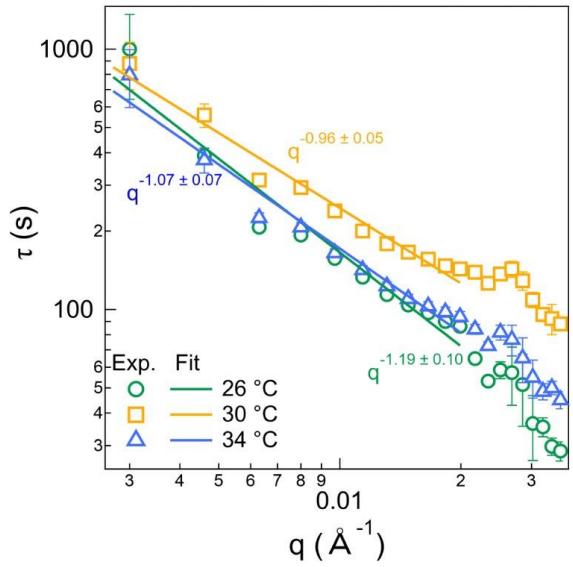

Figure 7 Wavevector dependence of relaxation time at 26 ˚C, 30 ˚C, and 34 ˚C. The relaxation time shows a power-law dependence $\tau \sim q^{-1}$. The exact slope of the linear region in the log-log plot is labeled in the figure. The error bars in the figure represent one standard deviation.

The observed faster dynamics at high-q by the XPCS supports our speculation that the increased water concentration favors faster particle dynamics in the particle domain. Combining all the results, the following physical picture is proposed to be the likely mechanism of the observed temperature dependence of the storage modulus. The rise of the storage modulus before reaching its maximum value is mainly due to the increase of interfacial tension between bicontinuous domains. It results from decreased miscibility since it becomes more thermodynamically unfavorable to mix the particle domain and the solvent domain upon heating. A previous study has revealed increased interfacial tension between water and 2,6-lutidine above the critical temperature.[41] The reduction of the storage modulus results from a more complete phase separation of the solvent in the particle domain. The particle surface favors water over lutidine. The water concentration is increased at higher temperatures. Both the decreased lutidine concentration and increased temperature reduce the solvent viscosity in the particle domain. It is thus easier for particles to move. Therefore, even though the interfacial tension keeps going up at higher

temperatures, the mechanical strength of the particle domain is weakened because of the decreased solvent viscosity at higher water concentrations and temperatures. It is noted that it has been reported that the viscosity of the water-rich phase in the phase-separated water/ 2,6-lutidine system decreases when increasing temperature. [41] Decreasing the lutidine concentration also reduces the viscosity. [45] The combined SANS and XPCS experimental results indicate that the competition of interfacial tension between domains and the solvent viscosity change in the particle domain results in a maximum value in storage modulus at intermediate temperatures. [41] The former increases the mechanical strength of the system when ramping up the temperature while the latter decreases the mechanical strength.

Conclusions

This work provides the first characterization of the rheological behavior of a model SeedGel system as a function of temperature. The storage modulus of the studied SeedGel is comparable to the strongest storage of modulus of Bijel systems. The rheological behavior of SeedGel shows good correlations with their static structures probed by SANS and dynamics characterized by XPCS.

This work also provides the first experimental verification that the macroscopic solvent phase separation indeed occurs at the gelation temperature in this model SeedGel system. It is the microscopic solvent phase separation that introduces the attraction between the particles to form the particle domain. The formation of the particle domain, in turn, helps arrest the macroscopic phase separation of the binary solvent. The SANS results indicate that the water concentration

continues to rise when increasing the temperature of the gel. The increased water concentration together with the higher temperature thus favors faster motions of particles in the particle domain.

The change in solvent composition surrounding the nanoparticles shows a huge impact on the dynamics of particles. The gel transition is driven by the glass transition of particles in the particle domain. The temperature with the slowest dynamics of particles exhibits the largest storage modulus. A relationship of $\tau \sim q^{-1}$ dependence is observed in the gel state, which is likely due to the internal stress as reported previously in a colloidal glass.

Acknowledgments

YX and YL acknowledge the financial support from Cooperative Agreement No. 70NANB12H239 and 70NANB10H256 of the National Institute of Standards and Technology (NIST), the U.S. Department of Commerce. YL acknowledges the support by the Center for High Resolution Neutron Scattering, a partnership between the National Institute of Standards and Technology and the National Science Foundation under Agreement No. DMR-2010792. AZ thanks for the funding from the Summer Undergraduate Research Fellowship (SURF) at NIST. The statements, findings, conclusions, and recommendations are those of the authors and do not necessarily reflect the view of NIST or the U.S. Department of Commerce. Identification of a commercial product does not imply recommendation or endorsement by NIST, nor does it imply that the product is necessarily the best for the stated purpose. This work benefited from the use of the SasView application, originally developed under NSF Award DMR - 0520547. SasView also contains code developed with funding from the EU Horizon 2020 program under the SINE2020 project Grant No 654000.

References:

1 B. Keshavarz, D. G. Rodrigues, J.-B. Champenois, M. G. Frith, J. Ilavsky, M. Geri, T. Divoux, G. H. McKinley and A. Poulesquen, *Proceedings of the National Academy of Sciences*, 2021, **118**, e2022339118.

2 H. Guo, S. Ramakrishnan, J. L. Harden and R. L. Leheny, *The Journal of Chemical Physics*, 2011, **135**, 154903.

3 D. Beysens and D. Estève, *Physical Review Letters*, 1985, **54**, 2123–2126.

4 D. Pontoni, T. Narayanan, J.-M. Petit, G. Grübel and D. Beysens, *Physical Review Letters*, 2003, **90**, 188301.

5 K. A. Macmillan, J. R. Royer, A. Morozov, Y. M. Joshi, M. Cloitre and P. S. Clegg, *Langmuir*, 2019, **35**, 10927–10936.

6 S. Manley, H. M. Wyss, K. Miyazaki, J. C. Conrad, V. Trappe, L. J. Kaufman, D. R. Reichman and D. A. Weitz, *Physical Review Letters*, 2005, **95**, 238302.

7 L. Bai, J. W. Fruehwirth, X. Cheng and C. W. Macosko, *Soft Matter*, 2015, **11**, 5282–5293.

8 Y. Xi, F. Zhang, Y. Ma, V. M. Prabhu and Y. Liu, *Nature Communications*, 2022, **13**, 3619.

9 Y. Xi, R. S. Lankone, L.-P. Sung and Y. Liu, *Nature Communications*, 2021, **12**, 910.

10 Y. Xi, J. B. Leão, Q. Ye, R. S. Lankone, L.-P. Sung and Y. Liu, *Langmuir*, 2021, **37**, 2170–2178.

11 C. Huang, J. Forth, W. Wang, K. Hong, G. S. Smith, B. A. Helms and T. P. Russell, *Nature Nanotechnology*, 2017, **12**, 1060–1063.

12 E. Koos and N. Willenbacher, *Science*, 2011, **331**, 897–900.

13 E. M. Herzig, K. A. White, A. B. Schofield, W. C. K. Poon and P. S. Clegg, *Nature Materials*, 2007, **6**, 966–971.

14 M. F. Haase, H. Jeon, N. Hough, J. H. Kim, K. J. Stebe and D. Lee, *Nature Communications*, 2017, **8**, 1234.

15 T. J. Thorson, E. L. Botvinick and A. Mohraz, *ACS Biomaterials Science & Engineering*, 2018, **4**, 587–594.

16 C. Jo, J. Hwang, W.-G. Lim, J. Lim, K. Hur and J. Lee, *Advanced Materials*, 2018, **30**, 1703829.

17 J.-M. Guenet, *Gels*, 2021, **7**, 65.

18 E. M. Herzig, K. A. White, A. B. Schofield, W. C. K. Poon and P. S. Clegg, *Nat Mater*, 2007, **6**, 966–971.

19 L. Li, C. Miesch, P. K. Sudeep, A. C. Balazs, T. Emrick, T. P. Russell and R. C. Hayward, *Nano Lett.*, 2011, **11**, 1997–2003.

20 D. Cai and P. S. Clegg, *Chemical Communications*, 2015, **51**, 16984–16987.

21 M. N. Lee, J. H. J. Thijssen, J. A. Witt, P. S. Clegg and A. Mohraz, *Advanced Functional Materials*, 2013, **23**, 417–423.

22 J. A. Witt, D. R. Mumm and A. Mohraz, *Soft Matter*, 2013, **9**, 6773.

23 K. A. Macmillan, J. R. Royer, A. Morozov, Y. M. Joshi, M. Cloitre and P. S. Clegg, *Langmuir*, 2019, **35**, 10927–10936.

24 J. A. Witt, D. R. Mumm and A. Mohraz, *Soft Matter*, 2013, **9**, 6773.

25 S. M. Melnikov, A. Höltzel, A. Seidel-Morgenstern and U. Tallarek, *Analytical Chemistry*, 2011, **83**, 2569–2575.

26 C. J. Glinka, J. G. Barker, B. Hammouda, S. Krueger, J. J. Moyer and W. J. Orts, *Journal of Applied Crystallography*, 1998, **31**, 430–445.

27 S. R. Kline, *Journal of Applied Crystallography*, 2006, **39**, 895–900.

28 D. Sheyfer, Q. Zhang, J. Lal, T. Loeffler, E. M. Dufresne, A. R. Sandy, S. Narayanan, S. K. R. S. Sankaranarayanan, R. Szczygiel, P. Maj, L. Soderholm, M. R. Antonio and G. B. Stephenson, *Physical Review Letters*, 2020, **125**, 125504.

29 Q. Zhang, E. M. Dufresne, S. Narayanan, P. Maj, A. Koziol, R. Szczygiel, P. Grybos, M. Sutton and A. R. Sandy, *Journal of Synchrotron Radiation*, 2018, **25**, 1408–1416.
30 Y. Jayalakshmi and E. W. Kaler, *Physical Review Letters*, 1997, **78**, 1379–1382.
31 M. N. Lee, J. H. J. Thijssen, J. A. Witt, P. S. Clegg and A. Mohraz, *Advanced Functional Materials*, 2013, **23**, 417–423.
32 J. A. Witt, D. R. Mumm and A. Mohraz, *Soft Matter*, 2013, **9**, 6773.
33 T. Domenech and S. S. Velankar, *Journal of Rheology*, 2017, **61**, 363–377.
34 A. P. R. Eberle, N. J. Wagner and R. Castañeda-Priego, *Physical Review Letters*, 2011, **106**, 1–4.
35 H. H. Winter and F. Chambon, *Journal of Rheology*, 1986, **30**, 367–382.
36 V. Trappe and D. A. Weitz, *Physical Review Letters*, 2000, **85**, 449–452.
37 B. Keshavarz, D. G. Rodrigues, J.-B. Champenois, M. G. Frith, J. Ilavsky, M. Geri, T. Divoux, G. H. McKinley and A. Poulesquen, *Proceedings of the National Academy of Sciences*, 2021, **118**, e2022339118.
38 R. G. Larson, *The Structure and Rheology of Complex Fluids*, Oxford University Press, 1999.
39 S. H. Sung, S. Kim, J. Hendricks, C. Clasen and K. H. Ahn, *Soft Matter*, 2018, **14**, 8651–8659.
40 R. Gupta, B. Baldewa and Y. M. Joshi, *Soft Matter*, 2012, **8**, 4171.
41 C. A. Grattoni, R. A. Dawe, C. Y. Seah and J. D. Gray, *Journal of Chemical & Engineering Data*, 1993, **38**, 516–519.
42 H. Guo, G. Stan and Y. Liu, *Soft Matter*, 2018, **14**, 1311–1318.
43 J. R. Villanueva-Valencia, H. Guo, R. Castañeda-Priego and Y. Liu, *Phys. Chem. Chem. Phys.*, 2021, **23**, 4404–4412.
44 C. E. Bertrand, P. D. Godfrin and Y. Liu, *The Journal of Chemical Physics*, 2015, **143**, 084704.
45 A. Stein, S. J. Davidson, J. C. Allegra and G. F. Allen, *The Journal of Chemical Physics*, 1972, **56**, 6164–6168.
46 D. Pontoni, T. Narayanan, J.-M. Petit, G. Grübel and D. Beysens, *Physical Review Letters*, 2003, **90**, 188301.
47 R. Dattani, E. F. Semeraro and T. Narayanan, *Soft Matter*, 2017, **13**, 2817–2822.
48 J. L. Harden, H. Guo, M. Bertrand, T. N. Shendruk, S. Ramakrishnan and R. L. Leheny, *The Journal of Chemical Physics*, 2018, **148**, 044902.
49 X. Lu, S. G. J. Mochrie, S. Narayanan, A. R. Sandy and M. Sprung, *Physical Review Letters*, 2008, **100**, 045701.
50 W. C. K. Poon, L. Starrs, S. P. Meeker, A. Moussaïd, R. M. L. Evans, P. N. Pusey and M. M. Robins, *Faraday Discussions*, 1999, **112**, 143–154.
51 A. Fluerasu, A. Moussaïd, A. Madsen and A. Schofield, *Physical Review E*, 2007, **76**, 010401.
52 R. A. Narayanan, P. Thiyagarajan, S. Lewis, A. Bansal, L. S. Schadler and L. B. Lurio, *Physical Review Letters*, 2006, **97**, 075505.
53 L. Cipelletti, S. Manley, R. C. Ball and D. A. Weitz, *Physical Review Letters*, 2000, **84**, 2275–2278.
54 L. Cipelletti, L. Ramos, S. Manley, E. Pitard, D. A. Weitz, E. E. Pashkovski and M. Johansson, *Faraday Discussions*, 2003, **123**, 237–251.
55 L. Hong, N. Smolin and J. C. Smith, *Physical Review Letters*, 2014, **112**, 158102.
56 Z. Wang, H. Guo, Y. Liu and X. Wang, *The Journal of Chemical Physics*, 2018, **149**, 084905.